# Numerical study of the mixture formation and stratified-flame-induced auto-ignition (SFI) combustion processes in a poppet-valve two-stroke direct injection gasoline engine

Bang-Quan He [a,*], Chang-Lin Lin [a], Xiao Li [a], Xinyan Wang [b], Hua Zhao [a,b], Yan Zhang [c]

[a] State Key Laboratory of Engines, Tianjin University, Tianjin 300072, PR China

[b] Centre for Advanced Powertrain and Fuels, Brunel University London, UK

[c] China North Engine Research Institute

**Abstract**: Two-stroke gasoline engines, as the substitutes of their four-stroke downsized counterparts, can mitigate knock, excessive thermal and mechanical loads for the improvement of fuel economy. But the combustion instability of the two-stroke gasoline engines at low loads is a dilemma. Flame propagation initiated by spark ignition combined with the auto-ignition of the mixture diluted by high residual gas fraction during flame propagation, i.e., stratified-flame-induced auto-ignition (SFI) combustion, is one possible solution to control ignition timing and improve combustion stability of a two-stroke direct injection spark ignition gasoline engine at low loads. To understand the relationships between the mixture formation and SFI combustion event, simulation was conducted at a fixed amount of fuel burned in a cycle. The results show that engine speed affects flame propagation and auto-ignition in the cylinder through the change in the distribution of fuel and residual gases. SFI combustion can occur during flame propagation at different engine speeds. With the increase of engine speed, increased fuel moves towards the spark plug while the temperature of the mixture around the cylinder increases with residual gases, leading to increased heat released by SFI auto-ignition. Although increased engine speed leads to a delay in ignition timing, shortened combustion duration increases indicated mean effective pressure.

**Keywords**: two-stroke; gasoline engine; engine speed; spark ignition; auto-ignition; simulation

* Corresponding Author. Tel.: +86 22 27406842 ext. 8011; fax: +86 22 27383362.
E-mail address: bqhe@tju.edu.cn (B.-Q. He).

## 1. Introduction

Compared with diesel engines, the thermal efficiencies of gasoline counterparts are much lower. Therefore, it is difficult for gasoline-powered passenger cars to meet the 2020 target of 95 g/km carbon dioxide ($CO_2$), equivalent to fuel consumption of around 4.1 l/100 km gasoline or 3.6 l/100km diesel. To reduce $CO_2$ emissions from four-stroke gasoline engines, various technologies have been investigated over the past decades. One is to downsize and boost in combination with direct injection in gasoline engines. Homogeneous charge compression ignition (HCCI) has the potential to simultaneously improve gasoline engines' fuel economy and decrease their nitrogen oxides ($NO_x$) emissions at part loads [1,2], due to rapid heat release and relatively low maximum combustion temperature [2,3]. A practical approach to achieve HCCI combustion in gasoline engines is to dilute mixture with residual gases through earlier exhaust valve closing timing before top dead centre (TDC) combined with later intake valve opening timing after TDC, i.e. negative valve overlap. However, HCCI combustion is dominated by chemical kinetics. Therefore, HCCI combustion phasing is difficult to be controlled. Relatively high hydrocarbon (HC) and carbon monoxide (CO) emissions are also concerns for HCCI engines at low loads and speeds [4,5] on account of low combustion temperature. In addition, HCCI combustion is restricted by severe knock or unacceptable pressure rise rate at high loads [6-8].

To effectively control the combustion phasing and decrease the maximum pressure rise rate of HCCI four-stroke gasoline engines, spark-assisted HCCI combustion or spark-assisted compression ignition (SACI) combustion was investigated [8,9]. In this context, flame propagation after spark ignition consumes part of the mixture in the cylinder and finally induces the auto-ignition of the unburned fuel in the cylinder [8]. Accordingly, spark-assisted HCCI combustion can partly solve the dependence on combustion phasing and peak heat release rate, and finally extend the upper load limit in HCCI combustion [10]. In the meantime, $NO_x$ emissions are relatively lower and thermal efficiency is higher in spark-assisted HCCI combustion compared to HCCI combustion [11] in the same conditions. To achieve auto-ignition temperature (~1050K), a large amount of heat released by flame propagation is required regardless of charge compositions [12,13]. It was found [14] that through controlling the quantity of fuel burned by flame propagation after spark ignition and charge temperature by adjusting the negative valve overlap, peak heat release rate can be decreased at a given combustion phasing.

However, spark ignition may improve the stability in HCCI four-stroke gasoline engines in some conditions while it has little or no effect in the others [15-19]. Lavoie et al. [20] found that the effectiveness

of spark ignition is the best at middle and high loads, due to relatively high flame speed, while it decreases at low loads, due to low flame speed. To raise the temperature of unburned mixture and alleviate the heat release in spark-assisted HCCI mode at part loads, charge stratification in the cylinder is one solution. In this case, flame speed in the cylinder plays an important role in the auto-ignition of the mixture diluted by residual gases [21]. With charge motion and gasoline direct injection, the relatively-rich mixture is formed around the cylinder centre while the lean mixture distributes around the cylinder. Thus, the early flame propagation is improved while the severe auto-ignition in the end gases is suppressed [22]. Dec et al. [23, 24] found that mixture stratification can effectively decrease the maximum pressure rise rate while it can enhance combustion efficiency at low loads. Ankit et al. [25] found that a high degree of temperature stratification in the cylinder can shorten ignition delay. Fuel-rich zones with low temperature have longer ignition delay relative to the fuel-lean ones with high temperature. However, auto-ignition is more sensitive to the stratification of temperature compared to that of fuel in the cylinder. Temperature stratification can mitigate the maximum heat release rate in HCCI engines while spark-ignition can precisely control the ignition timing in spark-assisted HCCI combustion mode [26]. Although spark-assisted HCCI combustion can solve some problems mentioned above, it can only be used in a narrow range over the entire speed-load map of a conventional spark ignition gasoline engine. Therefore, it is necessary to shift between conventional spark ignition and HCCI combustion at specific engine loads and speeds.

Although spark-assisted HCCI/SACI combustion can be used in four-stroke gasoline engines to extend the operating ranges with high thermal efficiency and low emissions, high pressure rise rate is still unacceptable at high loads. As a substitute of four-stroke operation, two-stroke operation is one solution to expand the operating load range towards high thermal efficiency at the same peak pressure rise rate, due to doubled firing frequency [27]. In the meantime, HCCI combustion can easily be achieved at low loads, due to high reactivity of the in-cylinder charge with high temperature [28]. On the other hand, excessive thermal and mechanical loads as well as knocking combustion in the aggressively downsized four-stroke gasoline engine can be reduced markedly in the case of two-stroke operation. However, conventional crankcase-scavenged two-stroke gasoline engines have inevitable charge losses and very high HC emissions, due to short-circuiting of fresh charge. Higher temperature and higher thermal stresses in the cylinder head and the piston crown also result in the durability problems of conventional crankcase-scavenged two-stroke gasoline engines. Therefore, poppet-valve two stroke direct injection gasoline

engines are interesting after considering scavenging efficiency, durability and acceptable permeability [29,30]. Recent simulation results show that dual spray injectors have the potential to increase the operating range of partially premixed combustion in a two-stroke gasoline engine and to decrease both noise and NOx emissions [31]. However, two-stroke gasoline engines feature high residual gases at idle and low loads. Combustion stability at these conditions is still a problem, due to high residual gas fraction with low temperature. HCCI combustion can be readily achieved in two-stroke gasoline engines at middle loads [32-34], due to relatively high exhaust temperature. External exhaust gas recirculation in combination with internal exhaust gas recirculation is the most effective approach to achieve HCCI combustion in two-stroke engines [35,36]. Accordingly, two-stroke gasoline engines have the potential to operate with high thermal efficiency [37], low exhaust emissions and high power-to-weight ratio [38-40] in the speed-load map operating in HCCI combustion.

Recently, stratified-flame-induced auto-ignition (SFI) combustion [41] was proposed to extend the operating range from high load to lower load in order to improve combustion stability and shorten combustion duration in a four-stroke gasoline engine. To reduce $NO_x$ and soot emission and increase thermal efficiency, partially premixed combustion (PPC) was experimentally investigated [42,43] and simulated [44,45] in the poppet-valve two-stroke diesel engines fueled with gasoline. However, the maximum in-cylinder pressure in PPC mode exceeds the limit that gasoline engines can tolerate and knock occurs at high loads. In a poppet-valve two-stroke gasoline engine, Nora and Zhao [34] found that 1.2 MPa indicated mean effective pressure (equivalent to 2.4 MPa in a four-stroke gasoline engine) with a peak pressure below 7 MPa can be achieved even at 800 rpm. However, the short time available for proper air-fuel mixing and scavenging inefficiency decrease the load at high speeds.

For two-stroke gasoline engines, inefficient scavenging results in high residual gas fraction in the cylinder at low loads, leading to combustion instability and high HC emissions. On the other hand, short time available for the preparation of air-fuel mixture also increases exhaust emissions. In the authors' previous study, it was found [47] that in the case of double fuel injection at fixed engine speed and a given cycle fuel injection quantity, the change in the second injection ratio alters the proportion of fuel burned through flame propagation and auto-ignition in the cylinder. But auto-ignition is difficult to occur when the second injection ratio is greater than 70%. In fact, engine speed is an important factor affecting residual gas fraction and fuel preparation. To control ignition timing through spark ignition and to improve the combustion stability of a two-stroke gasoline engine and increase its thermal efficiency at low loads, SFI

combustion may be a solution. However, to authors' knowledge, little literature about SFI combustion in the poppet-valve two-stroke gasoline engines can be found. The flow motion, the distribution of residual gases and fuel in the cylinder and the auto-ignition in the cylinder during flame propagation are influenced by engine speed and fuel injection strategy in a poppet-valve two-stroke direct injection gasoline engine. The objective of this study is to understand the temperature and composition distribution in the cylinder at different engine speeds in order to find their effect on flame propagation and SFI combustion in a poppet-valve two-stroke direct injection gasoline engine at a given amount of fuel burned in a cycle by means of three-dimensional (3D) computational fluid dynamics (CFD) simulation.

## 2. The combustion system of the two-stroke gasoline engine

The combustion system of the poppet-valve two-stroke direct injection gasoline engine consists in a pent-roof combustion chamber and a bowl in the piston as shown in Fig. 1. Two vertical intake ports coupled with a step structure in the pent-roof on the intake valve side are to form a reverse tumble flow in the cylinder during the intake stroke in order to reduce air short-circuiting and scavenge the exhaust gases in the combustion chamber during the valve overlap [48]. An outward-opening piezo-actuated direct injection injector and a spark plug are tilted installation near the cylinder centre in order to form ignitable mixture around the spark plug at the timing of spark ignition. Table 1 shows the specifications of the poppet-valve two-stroke direct injection gasoline engine. Fig.2 illustrates the valve lift profiles of the two-stroke gasoline engine. In the figure, BDC is bottom dead centre. During the scavenging process, the intake and exhaust valves are opened around BDC.

The meshes in the cylinder were automatically created by a 3D CFD software CONVERGE. The base mesh size of the combustion system was 4 mm. The local mesh size in the cylinder was automatically refined through adaptive mesh refinement (AMR) based on the gradient in the velocity and temperature during the simulation. The minimum mesh size generated by the AMR was 0.5 mm during the scavenging, compression and expansion processes. The mesh size around the intake and exhaust valves was 1 mm while it was 0.25 mm around the spark plug gap and the injector nozzle in order to calculate laminar flame after spark ignition. The meshes were in the range between 100,000 and 810,000 during the simulation.

## 3. Computation models

### *3.1. Spray models*

Although there are extensive stochastic phenomena in two-stroke spark ignition gasoline engines, this study only focuses on the ensemble-averaged flow motion and combustion processes. Therefore,

RANS model is chosen. In fact, RANS model can predict the stochastic phenomena during combustion process [49] and auto-ignition in the end gases [50]. To solve the turbulent vortex and viscidity of fluid with low Reynolds number and to improve the computational accuracy near combustion chamber wall, the RANS based realizable k–ε turbulence model [51] was used to simulate the flow in the cylinder. To effectively solve stochastic motion when turbulent vortex groups act on parcels, wall heat transfer was calculated with the O'Rourke model [52]. Spray development experiences several physical processes after the start of injection. Therefore, several spray sub-models used were shown in Table 2. In the modified KH-RT model, aerodynamic instabilities are responsible for the primary breakup of the liquid parent blobs while the secondary breakup of the child drops is the result of the competition between the KH and RT mechanisms. NTC model was adopted for the collisions of fuel droplets, due to higher computational accuracy and shorter calculation time relative to the O'Rourke model [60]. Different from Bai's model [61], Wall film model [58] for fuel wall impingement includes the interaction between liquid droplets and wall surface. The discrete multi-component model was used for each component during fuel vaporization. The spray behaviors were modeled by the Lagrangian parcel tracking method.

The surrogate of the gasoline with a research octane number of 93 is composed of 93% iso-octane and 7% n-heptane by volume.

*3.2. Combustion models*

There are different approaches to describe the flame front in the cylinder. The G-equation-based turbulent combustion model coupled with chemical kinetics can describe the combustion events of direct injection gasoline engines [62,63]. Therefore, a skeletal chemical kinetics mechanism [64] with 33 species for iso-octane and n-heptane was used to model fuel combustion in the cylinder. In this case, the flame front is defined as the boundary zone where G is zero. After the boundary zones of flame front in different crank angle are obtained, the direction of flame front propagation can be found. The combustion chamber is divided into unburned region prior to the flame front (G<0) and burned region after the flame front (G>0) [65].

The G-equation [66] is expressed as follows:

$$\frac{\partial \tilde{G}}{\partial t} + \left(\widetilde{\vec{v_f}} - \vec{v}_{vertex}\right) \cdot \nabla \tilde{G} = \frac{\overline{\rho_u}}{\bar{\rho}} s_t^0 \left|\nabla \tilde{G}\right| - D_t \tilde{k}_M \left|\nabla \tilde{G}\right| \quad (1)$$

where $\widetilde{G}$ is Favre-averaged G. $\widetilde{\vec{v_f}}$ is the Favre mean bulk fluid velocity in the flame front. $\vec{v}_{vertex}$ is the mesh vertex velocity. $\nabla \tilde{G}$ is the gradient of $\widetilde{G}$. $\overline{\rho_u}$ is the density of unburned mixture. $\bar{\rho}$ is the

mean gas density of turbulent flame. $D_t$ is turbulent diffusivity. $\tilde{k}_M$ is mean flame curvature. $s_t^0$ is turbulent flame speed.

$s_t^0$ is a function of laminar flame speed ($s_l^0$) and can be obtained in the following equation [67]:

$$s_t^0 = s_l^0 + v' \left\{ -\frac{a_4 b_3^2}{2b_1} D_a + \left[ \left( \frac{a_4 b_3^2}{2b_1} D_a \right)^2 + a_4 b_3^2 D_a \right]^{1/2} \right\} \quad (1)$$

where *v'* is turbulence intensity. $a_4$, $b_1$ and $b_3$ are constants derived from turbulence model. $D_a$ is the Damkohler number.

*3.3. Simulation validation*

For spray-guided direct injection gasoline engines, the distribution of mixture around the spark plug at the timing of spark ignition affects the development of initial flame kernel, flame propagation and combustion stability in the cylinder, especially in the exhaust-diluted mixture. Therefore, the simulation accuracy of spray and mixture formation in the cylinder is of great importance. To validate the simulation models mentioned above, experiments were carried out in a constant volume vessel and an engine test bench, respectively.

With Schlieren photography, the spray images at the fuel injection pressure of 10 MPa were recorded with a high-speed digital camera at 20000 frames per second in a constant volume vessel at the backpressure of 1 MPa, which was close to the average in-cylinder pressure during the second injection in this work. Based on the Zeuch method, the fuel injection rate was measured for simulation validation. Fig.3 shows the fuel injection rate with the time after the start of injection (ASOI).

After creating the meshes of the constant volume vessel, using the spray sub-models mentioned above and imputing fuel injection rate with time in the Converge software, the simulation results of spray development were obtained.

Fig.4 shows the experiment and simulation results of the spray. As shown in Fig.4 (a), the spray images of simulation and experiment are similar at the same ASOI. Since the experimental results of spray include the gas and liquid phase of fuel while their simulation results only show the liquid phase of fuel. Therefore, the experimental results of the shape and width of the spray tip have little different from those of simulation. It indicates that the simulation results of spray penetration and cone angles are in good agreement with those of experiments as shown in Fig.4 (b) and the spray models can predict the spray development in the engine.

After employing the validated spray sub-models and using the combustion models, in-cylinder

pressure and heat release rate were simulated. The simulation results of in-cylinder pressure and heat release rate were validated by the experiments obtained from a single cylinder poppet-valve two-stroke direct injection gasoline engine with a 81.6 mm bore, a 66.94 mm stroke and a 11.78 compress ratio operating at 1500 rpm and 3.6 bar indicated mean effective pressure in a previous study [47]. For the sake of brevity, the simulation results were not shown in this work.

*3.4 Simulation cases*

To realize SFI combustion in the two-stroke direct injection gasoline engine, split direct injection was adopted. The simulation cases were shown in Table 3. The engine speeds in the table are commonly used in two-stroke gasoline engines for vehicles [31,33,37]. To maintain high conversion efficiency of three-way catalytic converter, fuel/air equivalence ratio is at stoichiometry at different engine speeds. In the meantime, the fuel mass and spark timing (ST) were fixed in order to understand the combustion characteristics at different engine speeds. To keep equivalence fuel/air ratio constant, the mass of intake air per cycle is fixed and intake pressure is increased with engine speed. This is the reason why the volumetric efficiency in different cases was similar.

In Table 3, residual gas fraction (RGF) is the mass ratio of the residual gases to the total mixture including fresh air and the residual gases in the cylinder after the intake valves are closed. The start of the first direct injection ($SOI_1$) timing was at -110 °CA after top dead centre (ATDC) to form lean mixture diluted by residual gases in the cylinder. The start of the second injection ($SOI_2$) timing was at -40°CA ATDC to form relatively rich mixture around the spark plug and to facilitate the early development of flame kernel and flame propagation after spark ignition. The ratio of the second direct injection to the total ($r_{SOI2}$) was defined as the mass fraction of the second direct injection fuel to the total fuel injected in a cycle. During the simulation, $r_{SOI2}$ was 30% in order to understand the role of engine speed on mixture formation and subsequent combustion after spark ignition.

During the simulation, the inner surface temperatures of cylinder head, piston head and cylinder liner were 450 K, 450 K and 400 K, respectively. The intake and exhaust temperatures were 340 K and 690 K, respectively. With the GT-Power code, the initial mixture temperature and cylinder pressure were 1160 K and 0.294 MPa, respectively. The simulations started from exhaust valve opening (EVO) timing in the previous cycle to that in the following one.

**4. Results and discussion**

To quantitatively evaluate the distribution of fuel and temperature in the cylinder, the whole cylinder

is divided into several zones as shown in Fig.5. In the figure, the spark zone is defined as a sphere with 20 mm in diameter taking the midpoint of spark plug gap as the centre, since spark discharge can stretch up to 10 mm before restrike [68,69]. The combustible zones are the cells with equivalence ratio in the range of 0.6-2 and the velocity less than 15 m/s [69]. The centre zone is a cylindrical region with the diameter of 46 mm in the centre of the cylinder between cylinder head and piston crown. The region outside the centre zone is defined as the peripheral zone, in which the cell with temperature higher than 1050K and equivalence ratio in the range of 0.6-2 is called auto-ignition sites [70]. In the figure, the vertical clip plane S2 passes through spark plug and injector and plane S1 is the one passing through the spark plug and perpendicular to the plane S2.

*4.1 Mixture formation*

Engine speed affects flow motion, the time available for mixture preparation after fuel injection and subsequent combustion in the cylinder after spark ignition. A high engine speed usually leads to intensive flow motion in the cylinder [71], due to higher piston speed. The flow motion in the cylinder can be evaluated by turbulence kinetic energy ($\kappa$), i.e., the mean kinetic energy per unit mass associated with the eddies in turbulent flow. $\kappa$ can be obtained in the following turbulence kinetic energy transport equation [72]:

$$\frac{\partial \rho \kappa}{\partial t} + \frac{\partial \rho u_i \kappa}{\partial x_i} = \sigma_{ij} \frac{\partial u_i}{\partial x_j} + \frac{\partial}{\partial x_j} \frac{\mu}{Pr_{tke}} \frac{\partial \kappa}{\partial x_j} - \rho \varepsilon + S \tag{3}$$

where $\rho$ is the density of local fluid. $u_i$ is fluid velocity. $\sigma_{ij}$ is stress tensor. $\varepsilon$ is turbulent dissipation. $\mu$ is turbulent viscosity. $Pr_{tke}$ is Prandtl number. $S$ is source term. $t$ is time.

The average equivalence ratio ($\phi$), temperature and turbulence kinetic energy in the spark zone directly affect the formation of flame core and flame development after spark discharge. Fig.6 shows the variation of $\phi$, temperature and turbulence kinetic energy in the spark zone with crank angle.

As shown in Fig.6, after the first and second fuel injection, $\phi$ increases at first and then decreases. The main reason is that there is a reverse tumble flow generated by the vertical intake ports during the compression stroke and the injected fuel moves with the flow and finally enters the spark zone. On the other hand, fuel injection also produces a reverse flow as shown in Fig.7(b), which increases the amount of fuel in the spark zone. When fuel passes through the spark zone and moves away, the amount of fuel in the spark zone decreases. Therefore, $\phi$ increases first and then decreases after it reaches the peak. After -90°CA ATDC, the fuel is transported back to the spark zone with the reverse flow in the cylinder. As a

result, $\phi$ increases with crank angle. Furthermore, $\phi$ increases rapidly at 1000 rpm after around -80°CA ATDC since the time available for the mixing between air and fuel is longer and the mixture moves towards the spark zone. After the second fuel injection, the change of $\phi$ around the spark zone follows the same trend as that after the first fuel injection. With the increase of engine speed, the time available for the mixing between fuel and air in the spark zone decreases at the same crank angle duration. Therefore, $\phi$ in the spark zone is higher in long crank angle duration after the end of fuel injection at high engine speed.

In the meantime, the average temperature in the spark zone slightly goes down with increased crank angle after the first start of injection, due to fuel evaporative cooling in the cylinder. But it gradually increases, due to the compression from the ascending piston. The temperatures in the spark zone are close after the first fuel injection at different engine speeds. In addition, relatively high RGF as shown in Table 3 helps to increase the in-cylinder temperature at 2000 rpm. Although fuel evaporative cooling from the second injection still influences the in-cylinder temperature, the mass ratio of the second injection to the total is only 30%. Hence, its effect on the temperature decreases. However, after the timing of about -10°CA ATDC, the temperature in the spark zone decreases with engine speed at the same crank angle, due to slower flame propagation with high RGF and relatively-rich mixture around the spark zone, as will be discussed in detail later.

As expected, $\kappa$ in the spark zone increases with engine speed. The level of $\kappa$ decreases with crank angle since the reverse tumble breaks into vortexes and turbulence when the piston moves towards TDC. In addition, $\kappa$ increases during the first and the second fuel injection, due to the addition of fuel with high velocity. High $\kappa$ leads to high turbulence dissipation. Therefore, $\kappa$ attenuates significantly at high engine speed. High turbulence intensity promotes flame propagation while relatively-rich mixture in the spark zone also slows down the development of flame kernel. Therefore, the local flame speed in the spark zone is the competitive result of these two factors.

The interaction between fuel injection and reverse tumble flow influences the distribution of fuel and temperature in the cylinder. Fig. 7 shows the field of velocity and equivalence ratio of the mixture in the clip plane S1. In the figure, flow velocity vectors indicated by black arrows are superimposed in the images of velocity magnitudes. “IN” and “EX” stand for the sides of intake and exhaust valves, respectively.

As shown in Fig.7 (a), at -100°CA ATDC, a reverse tumble is formed in the cylinder centre regardless of engine speeds since the fresh charge from the vertical intake ports moves down along the cylinder wall and then goes upwards to the exhaust valves after it reaches the bowl in the piston head during the

scavenging processes. Thus, residual gases in the cylinder are swept out by fresh charge. The reverse tumble flow is further enhanced with the upwards-moving piston during the compression processes and then interacts with fuel spray. Therefore, the mixing process among fuel, air and residual gases is enhanced. As the piston moves towards TDC, the tumble flow breaks up and forms vortexes around -50°CA ATDC and finally dissipates at -30°CA ATDC.

Furthermore, after -100°CA ATDC, the velocity in the piston head bowl increases with increased engine speed, due to increased $k$ with engine speed as shown in Fig. 6. At -80°CA ATDC, the vortex centre of the tumble flow moves towards the right side of the cylinder while the flow with high velocity is around the spark zone at 2000 rpm. At -30°CA ATDC, there is still high velocity flow at 2000 rpm on the right side of the cylinder. It indicates that engine speed has important effect on the charge motion and the interaction between intake flow and combustion chamber changes the pattern of flow velocity distribution.

As shown in Fig.7 (b), the distribution of equivalence ratio is more complex relative to velocity since it is affected by fuel injection and charge motion in the cylinder. From -100°CA ATDC to -50°CA ATDC, the fuel from the first injection interacts with the reverse tumble flow regardless of the engine speed. Therefore, the fuel on the left side in the cylinder moves against the reverse tumble flow and goes back to the spark zone, leading to the increase of equivalence ratio around the spark zone. On the contrary, the fuel on the right side in the cylinder follows tumble flow and reaches the cylinder liner and then the piston head. At -100°CA ATDC, the fuel follows the tumble flow after the first fuel injection. But the equivalence ratio on the right side of the cylinder is higher than that on the left. The fuel on the left is blown away by the upward flow while the fuel on the right side follows the tumble flow generated during the intake stroke at different engine speeds. As a result, the fuel-rich mixture mainly distributes on the right side of the cylinder. Meanwhile, much fuel on the left side moves towards the spark zone at 2000 rpm, due to relatively high velocity of the upward flow motion near the spark plug as shown in Fig.7 (a). At -80°CA ATDC, the developed strong tumble flow transports the fuel on the right of the cylinder towards the piston head regardless of engine speed. At low engine speeds, more fuel-rich mixture distributes near piston head, due to relatively low local turbulence level for the mixing between fuel and air. At high engine speeds, the fuel-rich mixture is trapped at the bottom right corner of the cylinder, since there is less time available for the mixing of fuel and air. On the other hand, a part of fuel/air mixture on the left side follows the reverse tumble flow and reaches spark zone. At -50°CA ATDC, the mixture is relatively uniform in the cylinder centre, but the zone with high equivalence ratio in the lower left corner is large at 1000 rpm, due to lower

local turbulence level. At -30°CA ATDC, the fuel distribution from the second injection is quite different at different engine speeds. The rich mixture formed from the second injection is far from the spark plug at 1000 rpm while it is around the spark plug at a higher engine speed. The reason is that the stronger upward flow motion formed at a higher engine speed decreases the penetration of the injected fuel and moves the fuel from the second injection towards the spark plug while leaving relatively lean mixture in the periphery zone.

During the scavenging and compression processes, the in-cylinder hot residual gases mix with fresh air. When fuel is injected into the cylinder, it blends with the existing mixture there. Thus, the distribution of fuel and temperature in the cylinder changes with crank angle. In fact, simulation is carried out cell by cell in the cylinder. In this case, some cells in the cylinder have high residual gas fraction while the others have low. Therefore, residual gas fraction in a cell has important effect on the oxidation of fuel at the same conditions. To eliminate the effect of $CO_2$ and water ($H_2O$) in the residuals left from a previous cycle and in the burned gases during the combustion processes, a non-product equivalence ratio ($\varphi^{\#}$) is used to evaluate the mixture in a cell prior to flame front. $\varphi^{\#}$ is a dynamic parameter and can describe the variation of the local equivalence ratio in a cell, which is different from the average equivalence ratio in Fig.6. $\varphi^{\#}$ is calculated in the following equation [14,73]:

$$\varphi^{\#} = \frac{2C^{\#}_{-CO_2} + \frac{1}{2}H^{\#}_{-H_2O}}{O^{\#}_{-CO_2-H_2O}} \quad (4)$$

where $C^{\#}_{-CO2}$, $H^{\#}_{-H2O}$ and $O^{\#}_{-CO2-H2O}$ are the number of C, H and O atoms excluding those in the complete combustion products ($CO_2$ and $H_2O$). $\varphi^{\#}$ is one for a cell with stoichiometric mixture and is $\infty$ only for a cell only with fuel.

Although $\phi$ and $\varphi^{\#}$ have the same definition, $\varphi^{\#}$ can calculate the equivalence ratio in each cell during the engine operation cycle. Therefore, $\varphi^{\#}$ can effectively evaluate mixture combustion/auto-ignition in a cell. Fig.8 shows the distribution of $\varphi^{\#}$ and mixture temperature in the clip plane S1 at spark ignition timing (-20°CA ATDC). In the figure, the black isoline indicates that $\varphi^{\#}$ is one there.

As shown in Fig.8(a), $\varphi^{\#}$ distributions are affected by engine speed. With the increase of engine speed, the zone with high $\varphi^{\#}$ moves towards the cylinder centre. In the meantime, the isoline with $\varphi^{\#}$ =1 in the upper side gradually moves towards the spark plug and then leaves it, due to flow motion in the cylinder as discussed in Fig.7(b).

As shown in Fig.8(b), in-cylinder temperature is inhomogeneous at different engine speeds and the

zone with high temperature increases with engine speed since more fuel distributes around the cylinder centre as shown in Fig. 8(a). Higher temperature in the peripheral zone at high engine speed increases the reaction rate and facilitates the auto-ignition of the mixture if flammable mixture appears there, which is observed in Fig. 13.

To evaluate the effect of residual gases on the auto-ignition of mixture prior to flame front, dilution ratio ($\Phi_d$) is introduced and defined as follows:

$$\Phi_d = \frac{(RG)_{cell}}{(Air+Fuel+RG)_{cell}} \tag{5}$$

where $(RG)_{cell}$ is the mass of residual gas (RG) in a cell. $(Air+Fuel+RG)_{cell}$ is the total mass of air, fuel and RG in a cell.

Fig.9 shows the mass distribution of fuel-air mixture with temperature and $\varphi^{\#}$, and that with temperature and $\Phi_d$ at spark ignition timing. The fuel-air mixture is defined as the total mixture to be burned in the cylinder excluding the complete combustion products ($CO_2$, $H_2O$ and $N_2$). In the temperature-$\varphi^{\#}$ map, the increment steps of temperature and $\varphi^{\#}$ are 20 K and 0.05, respectively. In the temperature-$\Phi_d$ map, the increment steps of temperature and $\Phi_d$ is 10 K and 0.025, respectively. The white zone means the mass of fuel-air mixture is lower than 0.5 mg.

As shown in Fig.9 (a), the $\varphi^{\#}$ distribution gradually moves towards the high temperature region with engine speed, although the shapes of $\varphi^{\#}$ distribution are similar. It indicates that most fuel-air mixture has lower $\varphi^{\#}$ with higher temperature at different engine speeds. The main reason is that the evaporation of liquid fuels absorbs heat from the mixture and the charge cooling effect is low at the zones with low $\varphi^{\#}$. The mixture with high temperature and low $\varphi^{\#}$ may auto-ignite after spark ignition if it distributes in the peripheral zone prior to flame front.

As shown in Fig.9 (b), the zone of $\Phi_d$-temperature map and $\Phi_d$ distribution gradually increases with engine speed, since there is less time available for the mixing among fuel, air and residual gases in the cylinder. In the meantime, the region with the maximum mass gradually decreases with engine speed. Although residual gas fraction slightly increases with engine speed as shown in Table 3, engine speed has much effect on flow motion and the mixing of air and fuel. High dilution ratio means that little air and fuel is mixed with residual gases in a cell. Therefore, a cell with high dilution ratio and temperature indicates that little fuel is distributed there. This is the reason why the zone with high temperature is in the zones with low $\varphi^{\#}$ as shown in Fig. 9(a). Since there is long time for heat transfer through the wall of

combustion system during the same crank angle duration at low engine speed, the zone with high dilution ratio moves towards low temperature. Through the discussion above, it can be concluded that a cell with high temperature will appear when there is little fuel, high residual gas fraction and relatively low heat transfer through the wall of combustion system or low heat absorption from fuel.

*4.2 Stratified-flame-induced auto-ignition combustion*

Hydroxyl (OH) radical is an intermediate generated during hydrocarbon oxidation. It is dependent on local temperature and air/fuel equivalence ratio in the cylinder. OH radical can be used to evaluate auto-ignition during low temperature oxidation [74]. Based on the chemical reaction path analysis with the Chemkin software in this work, it is found that OH radical is mainly generated in the reaction $C_2H_3+H_2O \leftrightharpoons C_2H_4+OH$ in the temperature range of 900-1028 K before TDC, and the reactions $CO_2+H \leftrightharpoons CO+OH$ and $H_2O_2+M \leftrightharpoons OH+OH+M$ in the temperature range of 1050~2000K after TDC.

Heat release law (HRL), i.e., normalized integral heat release, can evaluate the heat release processes of an engine. Its definition is:

$$\mathrm{HRL} = \frac{(cumulative\ \ heat\ \ release)_{\theta}}{(cumulative\ \ heat\ \ release)_{total}} \tag{6}$$

Where, $(\text{cumulative heat release})_{\theta}$ is the cumulative heat release from spark ignition timing to a crank angle ($\theta$). $(\text{cumulative heat release})_{total}$ is the total cumulative heat release in a cycle.

To find the relationship between the mass of OH radical and HRL, Fig.10 shows the mass of OH radical in the peripheral zone prior to flame front and HRL as a function of crank angle at different speeds. Here, the mass of OH radical is the sum in each cell in the peripheral zone prior to flame front at a crank angle. It can be seen that HRL gradually increases before TDC regardless of engine speed. But it increases more rapidly at 1000 rpm relative to the other two engine speeds. The heat release is related to local temperature and equivalence ratio in the cylinder. At 2000 rpm, most fuel distributes in the cylinder centre while in the case of 1000 rpm and 1500 rpm, the fuel distributes in wider regions with appropriate equivalence ratio as shown in Fig. 8. Therefore, early development of flame kernel and flame propagation after spark ignition timing is slower at high engine speed and the early heat release rate at 2000 rpm is the lowest among these three engine speeds, leading to lower HRL at the early stage of flame propagation. After TDC, HRL almost linearly increases with crank angle at different engine speeds since the heat released through auto-ignition in the peripheral zone prior to flame front increases during flame propagation. After about 15ºCA ATDC, HRL gradually increases with crank angle since most fuel is

burned. During this period, flame propagation and auto-ignition occur simultaneously. Therefore, the more the mass of OH radical, the higher the HRL is. It indicates that auto-ignition in the peripheral zone prior to flame front can accelerate combustion.

On the other hand, the mass of OH radical in the peripheral zone prior to flame front gradually increases with crank angle before the TDC and its maximum is less than $10^{-4}$ mg at different speeds. But it is relatively lower than that after the TDC. The reason is that, during this period, little fuel is burned and OH radical is mainly generated in the reaction $C_2H_3+H_2O \leftrightharpoons C_2H_4+OH$ mentioned above. As a result, the mass of OH radical formed in the peripheral zone prior to flame front is lower. Moreover, the mass of OH radical in the peripheral zone before TDC decreases with the increase of engine speed at the same crank angle. It indicates that the oxidation of fuel in the cylinder is slower in the peripheral zone prior to flame front at a higher engine speed. However, the mass of OH radical rapidly increases after TDC with crank angle at different engine speeds. The reason is that, during this period, OH radical is from the reactions $CO_2+H \leftrightharpoons CO+OH$ and $H_2O_2+M \leftrightharpoons OH+OH+M$ mentioned above, due to increased temperature in the peripheral zone prior to flame front caused by flame propagation. Therefore, rapid increase in the mass of OH radical is observed. It can also be seen that the maximum mass of OH radical at 1500 rpm and 2000 rpm is higher than that at 1000 rpm after the TDC, which is attributed to the fact that more fuel is auto-ignited in the peripheral zones at higher engine speeds. In addition, the mass of OH radical at 2000 rpm is higher than that at 1500 rpm at the same crank angle after 5°CA ATDC since there are much lean mixture with low temperature in the peripheral zone at 2000 rpm. It means that more fuel auto-ignites in the peripheral zone prior to flame front at 2000 rpm and auto-ignition in the peripheral zone prior to flame front accelerates the processes of heat release in these conditions. After the mass of OH radical in the peripheral zone reaches its peak, it decreases with crank angle while HRL steadily increases, since the amount of unburned fuel left in the peripheral zone prior to flame front decreases while the unburned fuel left in the cylinder is still burning. Slow decrease of the mass of OH radical in the peripheral zone with crank angle at higher engine speed means that there are more unburned fuel left in the peripheral zone.

In the SFI mode, the low-temperature oxidation of the fuel/air mixture highly-diluted by residual gases in the unburned zone is enhanced by the heat released from the flame propagation and compression work by the up-moving piston, leading to the auto-ignition of the mixture in the peripheral zone prior to flame front. In this case, the higher the amount of the fuel burned through flame propagation, the less the amount of the fuel left for auto-ignition. Therefore, there is a transition point in the cumulative heat release

curve where the heat release mode is changed from pure flame propagation to the hybrid combustion mode in which both flame propagation and auto-ignition take place simultaneously. This transition point, i.e., auto-ignition timing (AIT) in this work, is defined as the crank angle when the mass fraction of OH radical in the peripheral zone prior to flame front is 0.002 [75]. AITs are marked with hollow points in Fig.10. It can be found that AITs are dependent on engine speed. The AIT at 1000 rpm is later than those at the other two engine speeds, since the in-cylinder temperature is lower in the former case, as shown in Fig.8. But the AIT at 2000 rpm is slightly later than that at 1500 rpm. In fact, the residual gases in the cylinder have thermal effect and dilution effect on the auto-ignition of mixture [28]. Although high RGF can increase in-cylinder temperature at the same amount of intake, residual gases also slows down the oxidation of fuel. Delayed auto-ignition timing at 2000 rpm means that the dilution effect of residual gases is the dominant factor compared to the thermal effect. After the AIT, the HRL increases sharply with the increase of engine speed, due to rapid increase of the heat released through auto-ignition in the peripheral zone prior to flame front. It can be inferred that auto-ignition in the peripheral zone prior to flame front accelerates heat release after AIT and the mass of OH radical in the peripheral zone prior to flame front can evaluate the level of auto-ignition in the cylinder.

Fig.11 shows indicated mean effective pressure (*IMEP*), the maximum pressure rise rate ($PRR_{max}$), the maximum cylinder pressure ($P_{max}$) and the fraction of the heat released by flame propagation before AIT ($HRF_{BAIT}$) as a function of engine speed. Here, $HRF_{BAIT}$ is defined as the ratio of the heat released by flame propagation before AIT to the total energy released in a cycle. It can be seen that with the increase of engine speed, *IMEP*, $PRR_{max}$ and $P_{max}$ increases while $HRF_{BAIT}$ decreases. Decreased $HRF_{BAIT}$ means that more fuel is burned through the combination of flame propagation and auto-ignition. Decreased negative compression work with delayed ignition timing combined with short combustion duration as shown in Fig. 12 leads to increased *IMEP*. $PRR_{max}$ and $P_{max}$ increase even at delayed ignition timing with increased engine speed as shown in Fig. 12, probably because lower heat transfer at higher speed contributes to the increase in $PRR_{max}$ and $P_{max}$. It indicates that rapid heat release rate plays a major role in the increase of $PRR_{max}$ and $P_{max}$ at a fixed amount of fuel burned in a cycle.

Ignition timing (CA10) and combustion duration can evaluate the combustion characteristics of an engine in different operating conditions. CA10 is defined as the crank angle at which 10% mass fraction of air-fuel mixture is burned. Combustion duration is the crank angles over which 10-90% mass fraction of fuel is burned. Fig. 12 shows the change of ignition timing and combustion duration with engine speed.

It can be found that with the increase of engine speed, the combustion duration shortens while ignition timing delays. Although the time available for the mixing among fuel, air and residual gases before spark timing is longer at 1000 rpm relative to the other two engine speeds at the same fuel injection timings, much fuel is distributed in the peripheral zone in the cylinder, leading to the decrease of temperature (Fig.8) on account of heat absorption by fuel evaporation from the surrounding. However, the $\varphi^{\#}$ in the spark zone is around 1 at 1000 rpm while it is fuel-rich zone at 1500 rpm and 2000 rpm as shown in Fig.8. As a result, it is helpful to the development of initial flame kernel and flame propagation at 1000 rpm and the initial phase for CA10 in terms of crank angle is shorter at 1000 rpm. In the meantime, the mixture with relatively low temperature around the cylinder wall cannot easily auto-ignite. This in turn leads to longer combustion duration at 1000 rpm. At high engine speed, the in-cylinder dilution ratio is increased and the fuel-rich mixture mainly concentrates around the spark zone. Therefore, the flame propagation slows down and CA10 delays. Although the amount of the heat released by flame propagation is less at high engine speed, the mixture with high temperature around the cylinder wall (Fig.8) readily auto-ignites. As a result, the combustion duration is shortened at high engine speeds. Short combustion duration indicates that the subsequent auto-ignition of the exhaust-diluted mixture in the peripheral zone after flame propagation accelerates the entire combustion process.

In the SFI mode, the flame propagation affects the thermal states of the unburned mixture in the peripheral zone and finally changes the history of auto-ignition there. Fig.13 shows the top view of the temperature distribution and the location of flame front in the cylinder. In the figure, the red iso-surface with G=0 represents the flame front. The auto-ignition zones prior to flame front are defined as the cells with temperature higher than 1050 K and $\varphi^{\#}$ in the range between 0.6 and 1.6.

It can be seen in Fig.13 (a) that at AIT, the temperature in the auto-ignition zones prior to flame front is relatively lower than that of the flame front surface. For the same reason mentioned above, the burned zone by flame propagation decreases with engine speed since the initial phase is laminar in nature, and for a given propagation time, less crank angle is used. On the other hand, increased dilution ratio and decreased combustible mixture around the cylinder with engine speed also decrease flame propagation speed. It is also seen that the flame propagation speed is different in different directions. The main reason is that the tilted injector causes inhomogeneous fuel distribution in the cylinder and the turbulent flow with different scales in the cylinder also produces uneven distribution of mixture. It means that RANS model can capture the features of combustion in the cylinder. Pomraning et al. [76] found that employing

fine mesh to RANS simulation can accurately predict combustion results. On the other hand, auto-ignition also depends on the engine speed, which is attributed to uneven temperature and mixture distribution. The auto-ignition zones at 2000 rpm are larger than those at 1000 rpm and 1500 rpm, due to higher initial temperature from the heating of residual gases.

At 10°CA ATDC in Fig.13(b), a large amount of mixture is consumed by flame propagation and only a small amount of mixture in the peripheral zone auto-ignites at 1000 rpm. However, at 1500 rpm and 2000 rpm, the mixture in the cylinder is mainly consumed by auto-ignition while the burned regions by flame propagation change little, due to slow flame propagation speeds. In addition, the auto-ignition occurs at different sites in the cylinder, and the corresponding temperature of the auto-ignition zones increases with crank angle at different engine speeds. The large zones with the temperature around 2200K prior to flame front result in the peak of OH radical as shown in Fig.10.

At 20°CA ATDC in Fig.13(c), the flame front almost reaches the cylinder wall at 1000 rpm, while it is still in the cylinder centre at 2000 rpm. Flame propagation is mainly dependent on turbulence, local air/fuel equivalence ratio, temperature and residual gas fraction. It indicates that flame cannot propagate in the mixture diluted by residual gases and the fuel in the peripheral zone prior to flame front can only be consumed through auto-ignition at 2000 rpm. Therefore, how to achieve the auto-ignition in the zones where flame cannot propagate is important to increase the thermal efficiency of an engine in SFI mode.

**5. Conclusions**

To achieve stable combustion and shortened combustion duration in a poppet-valve two-stroke gasoline engine at low loads with high residual gas fraction, auto-ignition in exhaust-diluted mixture in the peripheral zones induced by flame propagation with spark ignition was proposed and simulated at fixed amount of fuel burned in a cycle at different engine speeds. The effect of engine speed on fuel distribution, flame propagation and auto-ignition in the cylinder was discussed. The following conclusions can be drawn:

- With the increase of engine speed, the fuel injected into the cylinder is concentrated around the spark plug, leading to fuel-rich mixture in the spark zone and high temperature mixture in the peripheral zone.
- Stratified-flame-induced auto-ignition combustion can occur during flame propagation at different engine speeds. But the zones and mass of the fuel burned through auto-ignition are dependent on engine speed. High engine speed leads to slow flame propagation with high dilution level and over-

rich mixture around the spark zone. However, the amount of the mixture with high temperature in the peripheral zone increases. Therefore, increased engine speed results in increased heat released through auto-ignition. OH radical can be used to evaluate the occurrence of auto-ignition in the unburned mixture in the cylinder.

- SFI combustion can shorten combustion duration with the increase of engine speed although the onset of combustion delays. However, IMEP steadily increases, which indicates that SFI combustion can improve thermal efficiencies of the engine in these conditions.

**Acknowledgements**

The authors would like to acknowledge the financial support by the Ministry of Science and Technology (MOST) through the 973 project Grant number 2013CB228403 and the National Natural Science Foundation of China through the projects of Grant number 51606175 and 51476151.

**References**

[1] H. Zhao, J. Li, Performance and analysis of a 4-stroke multi-cylinder gasoline engine with CAI combustion, SAE Paper 2002-01-0420.

[2] J. Li, H. Zhao, N. Ladommatos, T. Ma, Research and development of controlled autoignition (CAI) combustion in a 4-stroke multi-cylinder gasoline engine, SAE Paper 2001-01-3608.

[3] R.H. Stanglmaier, C.E. Roberts, Homogeneous charge compression ignition (HCCI): benefits, compromises, and future engine applications, SAE Paper 1999-01-3682.

[4] J.E. Dec, Advanced compression-ignition engines-understanding the in-cylinder processes, P. Combust. Inst. 32(2)(2009)2727-2742.

[5] R. Dahms, C. Felsch, O. Röhl, N. Peters, Detailed chemistry flamelet modeling of mixed-mode combustion in spark-assisted HCCI engines, P. Combust. Inst. 33(2) (2011)3023-3030.

[6] J.E. Dec, Y. Yang, Boosted HCCI for high power without engine knock and with ultra-low NOx emissions-using conventional gasoline, SAE Paper 2010-01-1086.

[7] H. Xie, L. Li, T. Chen, W. Yu, X. Wang, H. Zhao, Study on spark assisted compression ignition (SACI) combustion with positive valve overlap at medium-high load, Appl. Energ. 101 (2013)622-633.

[8] B.T. Zigler, P.E. Keros, K.B. Helleberg, M. Fatouraie, D. Assanis, M.S. Wooldridge, An experimental investigation of the sensitivity of the ignition and combustion properties of a single-cylinder research engine to spark-assisted HCCI, Int. J. Engine Res. 12(4) (2011) 353-375.

[9] Z. Wang, J. Wang, S. Shuai, G. Tian, X. An, Q. Ma, Study of the effect of spark ignition on gasoline

HCCI combustion, P. I. Mech. Eng. D-J. Aut. 220(6) (2006) 817-825.

[10] Z. Wang, X. He, J. Wang, S. Shuai, F. Xu, D. Yang, Combustion visualization and experimental study on spark induced compression ignition (SICI) in gasoline HCCI engines, Energ. Convers. Manage. 51(5) (2010) 908-917.

[11] L. Manofsky, J. Vavra, D.N. Assanis, A. Babajimopoulos, Bridging the gap between HCCI and SI: spark assisted compression ignition, SAE Paper 2011-01-1179.

[12] L.M. Olesky, J.B. Martz, G.A. Lavoie, J. Vavra, D.N. Assanis, A. Babajimopoulos, The effects of spark timing, unburned gas temperature, and negative valve overlap on the rates of stoichiometric spark assisted compression ignition combustion, Appl. Energ. 105 (2013) 407-417.

[13] L.M. Olesky, G.A. Lavoie, D.N. Assanis, M.S. Wooldridge, J.B. Martz, The effects of diluent composition on the rates of HCCI and spark assisted compression ignition combustion, Appl. Energ. 124 (2014) 186-198.

[14] R.J. Middleton, L.M. Olesky, G.A. Lavoie, M.S. Wooldridge, D.N. Assanis, J.B. Martz, The effect of spark timing and negative valve overlap on spark assisted compression ignition combustion heat release rate, P. Combust. Inst. 35(3) (2015) 3117-3124.

[15] A. Babajimopoulos, D. Assanis, D. Flowers, S. Aceves, R. Hessel, A fully coupled computational fluid dynamics and multi-zone model with detailed chemical kinetics for the simulation of premixed charge compression ignition engines, Int. J. Engine Res. 6(5) (2005) 497-512.

[16] J. Hyvönen, G. Haraldsson, B. Johansson, Operating conditions using spark assisted HCCI combustion during combustion mode transfer to SI in a multi-cylinder VCR-HCCI engine, SAE Paper 2005-01-0109.

[17] H. Persson, M. Agrell, J.O. Olsson, B, Johansson, H. Ström, The effect of intake temperature on HCCI operation using negative valve overlap, SAE Paper 2004-01-0944.

[18] H. Persson, R. Pfeiffer, A. Hultqvist, B. Johansson, H. Ström, Cylinder-to-cylinder and cycle-to-cycle variations at HCCI operation with trapped residuals, SAE Paper 2005-01-0130.

[19] R.M. Wagner, K.D. Edwards, C.S. Daw, J.B. Green, B.G. Bunting, On the nature of cyclic dispersion in spark assisted HCCI combustion, SAE Paper 2006-01-0418.

[20] G.A. Lavoie, J. Martz, M. Wooldridge, D. Assanis, A multi-mode combustion diagram for spark assisted compression ignition, Combust. Flame 157(6) (2010) 1106-1110.

[21] X. Wang, H. Zhao, H. Xie, B.Q. He, Numerical study of the effect of piston shapes and fuel injection

strategies on in-cylinder conditions in a PFI/GDI gasoline engine, SAE Paper 2014-01-2670.

[22] K. Yoshizawa, A. Teraji, H. Miyakubo, K. Yamaguchi, T. Urushihara, Study of high load operation limit expansion for gasoline compression ignition engines, ASME Paper ICES 2003-0543.

[23] J.E. Dec, M. Sjöberg, A parametric study of HCCI combustion-the sources of emissions at low loads and the effects of GDI fuel injection, SAE Paper 2003-01-0752.

[24] W. Hwang, J.E. Dec, M. Sjöberg, Fuel stratification for low-load HCCI combustion: performance & fuel-PLIF measurements, SAE Paper 2007-01-4130.

[25] A. Bhagatwala, J.H. Chen, T. Lu, Direct numerical simulations of HCCI/SACI with ethanol, Combust. Flame 161(7) (2014)1826-1841.

[26] C.S. Yoo, Z. Luo, T. Lu, H. Kim, J.H. Chen, A DNS study of ignition characteristics of a lean iso-octane/air mixture under HCCI and SACI conditions, P. Combust. Inst. 34(2) (2013)2985-2993.

[27] R.J. Osborne, J. Stokes, T.H. Lake, P.J. Carden, J.D. Mullineux, L.R. Helle, et al, Development of a two-stroke/four-stroke switching gasoline engine-the 2/4 SIGHT concept, SAE Paper 2005-01-1137.

[28] J. Javier López, S. Molina, A. García, J. Valero-Marco, F. Justet, Analysis of the potential of a new automotive two-stroke gasoline engine able to operate in spark ignition and controlled autoignition combustion modes, Appl. Therm. Eng. 126(2017) 834-847.

[29] P. Tribotte, F. Ravet, V. Dugue, P. Obernesser, N. Quechon, J. Benajes, et al, Two strokes diesel engine-promising solution to reduce $CO_2$ emissions, Procedia-Social Behavioral Sciences 48(2012)2295-2314.

[30] J. Benajes, R. Novella, D.D. Lima, P. Tribotté, N. Quechon, P. Obernesser, et al, Analysis of the combustion process, pollutant emissions and efficiency of an innovative 2-stroke HSDI engine designed for automotive applications, Appl. Therm. Eng. 58(1) (2013)181-193.

[31] A. Broatch, R. Novella, J. García-Tíscar, J. Gomez-Soriano, Potential of dual spray injectors for optimising the noise emission of gasoline partially premixed combustion in a 2-stroke HSDI CI engine, Appl. Therm. Eng. 134(2018) 369-378.

[32] Y. Zhang, H. Zhao, M. Ojapah, A. Cairns, Effects of injection timing on CAI operation in a 2/4-stroke switchable GDI engine, SAE Paper 2011-01-1776.

[33] Y. Zhang, H. Zhao, M. Ojapah, A. Cairns, Experiment and analysis of a direct injection gasoline engine operating with 2-stroke and 4-stroke cycles of spark ignition and controlled auto-ignition combustion, SAE Paper 2011-01-1774.

[34] M.D. Nora, H. Zhao, High load performance and combustion analysis of a four-valve direct injection gasoline engine running in the two-stroke cycle, Appl. Energ. 159(2015)117-131.

[35] A.M. Andwari, A.A. Aziz, M.F.M. Said, Z.A. Latiff, Experimental investigation of the influence of internal and external EGR on the combustion characteristics of a controlled auto-ignition two-stroke cycle engine, Appl. Energ. 134(2014)1-10.

[36] A.M. Andwari, A.A. Aziz, F.M.M. Said, Z.A. Latiff, An experimental study on the influence of EGR rate and fuel octane number on the combustion characteristics of a CAI two-stroke cycle engine, Appl. Therm. Eng. 71(1) (2014)248-258.

[37] Y. Zhang, H. Zhao, Investigation of combustion, performance and emission characteristics of 2-stroke and 4-stroke spark ignition and CAI/HCCI operations in a DI gasoline, Appl. Energ. 130 (2014) 244-255.

[38] M.A. Amin, A.A. Azhar Homogenous charge compression ignition (HCCI) technique: a review for application in two-stroke gasoline engines, Appl. Mech. Mater. 165(2012)53-57.

[39] U. Asad, M .Zheng, Exhaust gas recirculation for advanced diesel combustion cycles, Appl. Energ. 123 (2014) 242-252.

[40] M. Fathi, R.K. Saray, M.D. Checkel, The influence of exhaust gas recirculation (EGR) on combustion and emissions of n-heptane/natural gas fueled homogeneous charge compression ignition (HCCI) engines, Appl. Energ. 88(12)(2011)4719-4724.

[41] X. Wang, H. Zhao, H. Xie, Effect of piston shapes and fuel injection strategies on stoichiometric stratified flame ignition (SFI) hybrid combustion in a PFI/DI gasoline engine by numerical simulations, Energ. Convers. Manage. 98(2015)387-400.

[42] J. Benajes, R. Novella, D.D. Lima, P. Tribotte, Investigation on multiple injection strategies for gasoline PPC operation in a newly designed 2-stroke HSDI compression ignition engine, SAE Paper 2015-01-0830.

[43] J. Benajes, J. Martín, R. Novella, K. Thein, Understanding the performance of the multiple injection gasoline partially premixed combustion concept implemented in a 2-Stroke high speed direct injection compression ignition engine, Appl. Energ. 161(2016) 465-475.

[44] J. Benajes, R. Novella, D.D. Lima, P. Tribotté, Analysis of combustion concepts in a newly designed two-stroke high-speed direct injection compression ignition engine, Int. J. Eng. Res. 161 (2015)52-67.

[45] J. Benajes, R. Novella, D.D. Lima, P. Tribotté, N. Quechon, P. Obernesser, et al, Analysis of the combustion process, pollutant emissions and efficiency of an innovative 2-stroke HSDI engine designed for automotive applications, Appl. Therm. Eng. 58(2013)181-193.

[46] M.D. Nora, H. Zhao, High load performance and combustion analysis of a four-valve direct injection gasoline engine running in the two-stroke cycle, Appl. Energ. 159(2015)117-131.

[47] B.Q. He, C.L. Lin, Numerical study of the effect of injection strategies on SFI hybrid combustion process on a poppet-valve two-stroke DI gasoline engine, Trans. CSICE 38(5) (2017)406-414.

[48] Z.H. Li, B.Q. He, H. Zhao, Influences of intake ports and pent-roof structures on the flow characteristics of a poppet-valved two-stroke gasoline engine, Int. J. Engine Res. 17(10) (2016)1077-1091.

[49] R. Scarcelli, J. Sevik, T. Wallner, K. Richards, E. Pomraning, P.K. Senecal, Capturing cyclic variability in exhaust gas recirculation dilute spark-ignition combustion using multicycle RANS, J. Eng. Gas Turbines Power 138(11)(2016)112803.

[50] A. D'Adamo, S. Breda, S. Fontanesi, A. Irimescu, S. Merola, C. Tornatore, A RANS knock model to predict the statistical occurrence of engine knock, Appl. Energ. 191 (2017) 251-263.

[51] Z. Han, R.D. Reitz, Turbulence modeling of internal combustion engines using RNG κ-ε models, Combust. Sci. Technol. 106(4-6)(1995)267-295.

[52] A.A. Amsden, KIVA-3V: A block-structured KIVA program for engines with vertical or canted valves, Los Alamos National Lab, NM (United States), 1997.

[53] R.D. Reitz, R. Diwakar, Structure of high-pressure fuel sprays, SAE Paper 870598.

[54] R.D. Reitz, F.V. Bracco, Mechanisms of breakup of round liquid jets. In: N. Cheremisnoff (Ed.), The Encyclopedia of Fluid Mechanics, Gulf Publishing, Houston, Texas, 1986, pp. 233-249.

[55] J. Xin, L. Ricart, R.D. Reitz, Computer modeling of diesel spray atomization and combustion, Combust. Sci. Technol. 137(1-6) (1998)171-194.

[56] A.B. Liu, D. Mather, R.D. Reitz, Modeling the effects of drop drag and breakup on fuel sprays, SAE Paper 930072.

[57] D.P. Schmidt, C.J. Rutland, A new droplet collision algorithm, J. Comput. Phys. 164(1) (2000) 62-80.

[58] D.M. Gonzalez, Z. Lian, R.D. Reitz, Modeling diesel engine spray vaporization and combustion, SAE Paper 920579.

[59] Y. Ra, R.D. Reitz, A vaporization model for discrete multi-component fuel sprays, Int. J. Multiphas. Flow 35(2) (2009)101-117.

[60] P.J. O'Rourke, A.A. Amsden, A spray/wall interaction submodel for the KIVA-3 wall film model, SAE Paper 2000-01-0271.

[61] C. Bai, A.D. Gosman, Development of methodology for spray impingement simulation, SAE Paper 950283.

[62] L. Liang, R.D. Reitz, C.O. Iyer, J. Yi, Modeling knock in spark-ignition engines using a G-equation combustion model incorporating detailed chemical kinetics, SAE Paper 2007-01-0165.

[63] S. Singh, R.D. Reitz, D. Wickman, D. Stanton, Z. Tan, Development of a hybrid auto-ignition/ flame-propagation model and validation against engine experiments and flame lift off, SAE Paper 2007-01-0171.

[64] T. Tsurushima, A new skeletal PRF kinetic model for HCCI combustion, P. Combust. Inst. 32(2) (2009) 2835-2841.

[65] Z. Tan, R.D. Reitz, Modeling ignition and combustion in spark-ignition engines using a level set method, SAE Paper 2003-01-0722.

[66] Z. Tan, S.C. Kong, R.D. Reitz, Modeling premixed and direct injection SI engine combustion using the G-equation model, SAE Paper 2013-01-1843.

[67] N. Peters, Turbulent combustion, Cambridge University Press, Cambridge, 2000.

[68] M.C. Drake, T.D. Fansler, A.M. Lippert, Stratified-charge combustion: modeling and imaging of a spray-guided direct-injection spark-ignition engine, P. Combust. Inst. 30(2) (2005)2683-2691.

[69] R. Dahms, T.D. Fansler, M.C. Drake, T.W. Kuo, A.M. Lippert, N. Peters, Modeling ignition phenomena in spray-guided spark-ignited engines, P. Combust. Inst. 32(2) (2009) 2743-2750.

[70] J.B. Martz, H. Kwak, H.G. Im, D.N. Assanis, Combustion regime of a reacting front propagating into an auto-igniting mixture, P. Combust. Inst. 33(2) (2011)3001-3006.

[71] A.S. Krishna, J.M. Mallikarjuna, D. Kumar, Effect of engine parameters on in-cylinder flows in a two-stroke gasoline direct injection engine, Appl. Energ.176(2016)282-294.

[72] J.B. Heywood, Internal combustion engine fundamentals, Mcgraw-hill, New York, 1988.

[73] J.B. Martz, R.J. Middleton, G.A. Lavoie, A. Babajimopoulos, D.N. Assanis, A computational study and correlation of premixed isooctane air laminar reaction fronts diluted with EGR, Combust. Flame 159(10) (2012)3146-3157.

[74] N. Kawahara, E. Tomita, Y. Sakata, Auto-ignited kernels during knocking combustion in a spark-ignition engine, P. Combust. Inst. 31(2) (2007)2999-3006.

[75] J. Pan, H. Wei, G. Shu, M. Pan, D. Feng, and N. Li, Les analysis for auto-ignition induced abnormal combustion based on a downsized SI engine. Appl. Energ. 191(2017)183-192.

[76] E. Pomraning, K. Richards, P. Senecal, Modeling turbulent combustion using a RANS model, detailed chemistry, and adaptive mesh refinement, SAE Paper 2014-01-1116.

## List of Tables

Table 1 Engine specifications.

| | |
|---|---|
| Bore | 82 mm |
| Stroke | 67 mm |
| Displacement | 0.35 L |
| Compression ratio | 11.86 |
| Injector | Piezo-actuated |

Table 2 Sub-models for spray simulation.

| Items | Models |
|---|---|
| Drop turbulent dispersion | O'Rourke [52] |
| Parcel distribution | Blob injection [53] |
| Spray breakup | KH-RT [54,55] |
| Drop drag | Dynamic drag [56] |
| Collision | NTC [57] |
| Drop/wall interaction | Wall film [58] |
| Evaporation | Multi-component vaporization [59] |

Table 3 Simulation conditions.

| Cases | 1 | 2 | 3 |
|---|---|---|---|
| Engine speed | 1000 rpm | 1500 rpm | 2000 rpm |
| Intake pressure | 0.104 MPa | 0.107 MPa | 0.109 MPa |
| Air mass per cycle | 144 mg | 144 mg | 144 mg |
| Residual gas fraction | 32.1 % | 34.7 % | 36.7 % |
| Volumetric efficiency | 42.9% | 42.5% | 42.1% |
| Fuel mass per cycle | 9.6 mg | 9.6 mg | 9.6 mg |
| Fuel/air equivalence ratio | 1 | 1 | 1 |
| Start of the first direct injection after TDC | -110 °CA | -110 °CA | -110 °CA |
| Start of the second direct injection after TDC | -40 °CA | -40 °CA | -40 °CA |
| Ratio of the second direct injection to the total | 30% | 30% | 30% |
| Spark timing after TDC | -20 °CA | -20 °CA | -20 °CA |

## List of Figures

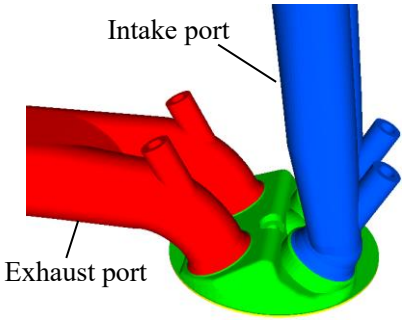


Fig. 1. Schematic of the engine combustion system.

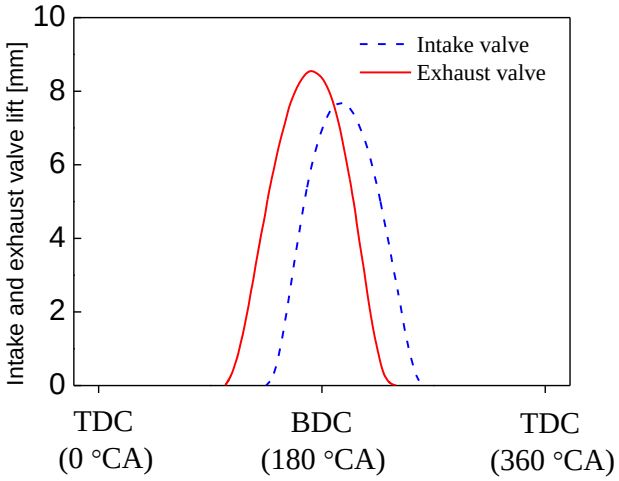


Fig. 2. Valve lift profiles of the two-stroke gasoline engine.

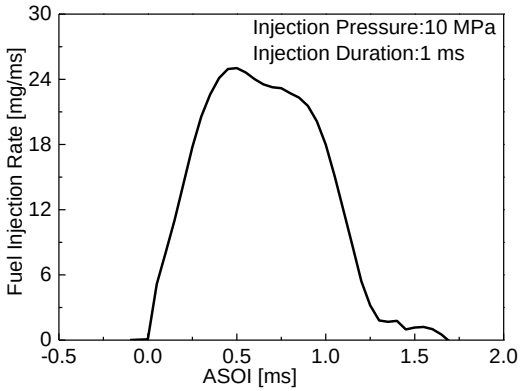


Fig. 3. Fuel injection rate of the outward-opening piezo-actuated direct injection injector.

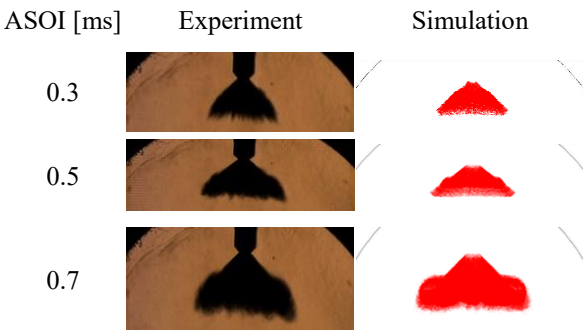


(a)

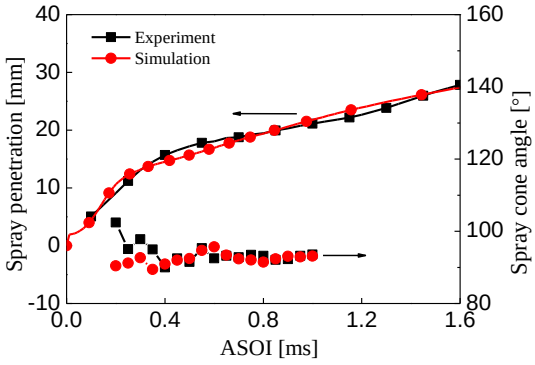


(b)

Fig. 4. Comparison of spray shape (a) and penetration and cone angle (b) between experiment and simulation at the backpressure of 1 MPa.

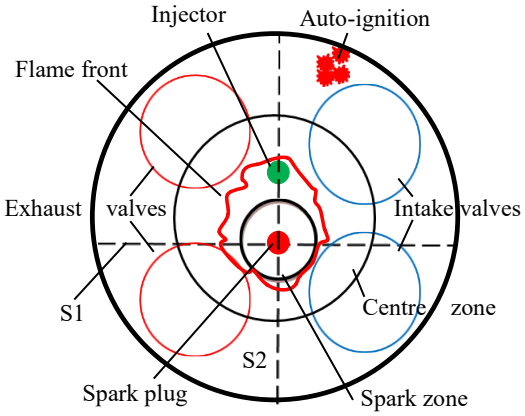


Fig. 5. The definition of various zones in the cylinder.

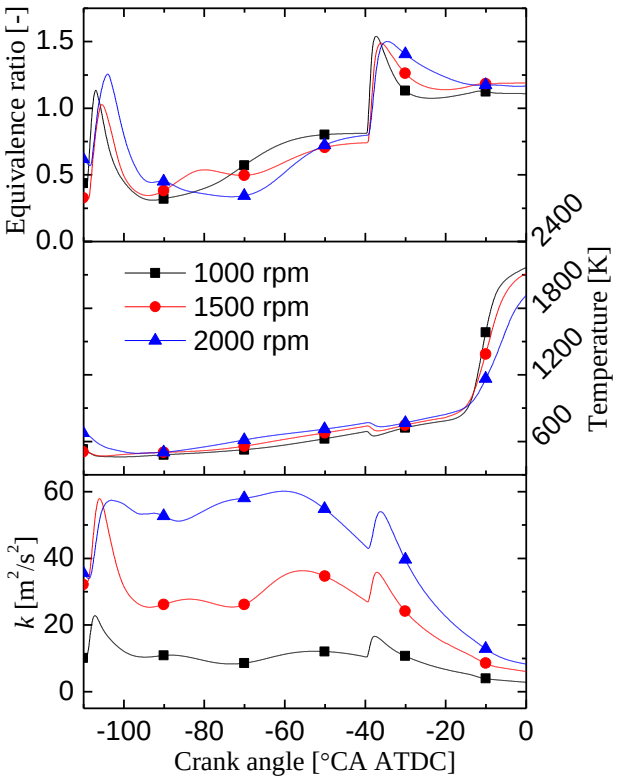


Fig. 6. The variation of equivalence ratio, temperature and $\kappa$ of the mixture in the spark zone with crank angle.

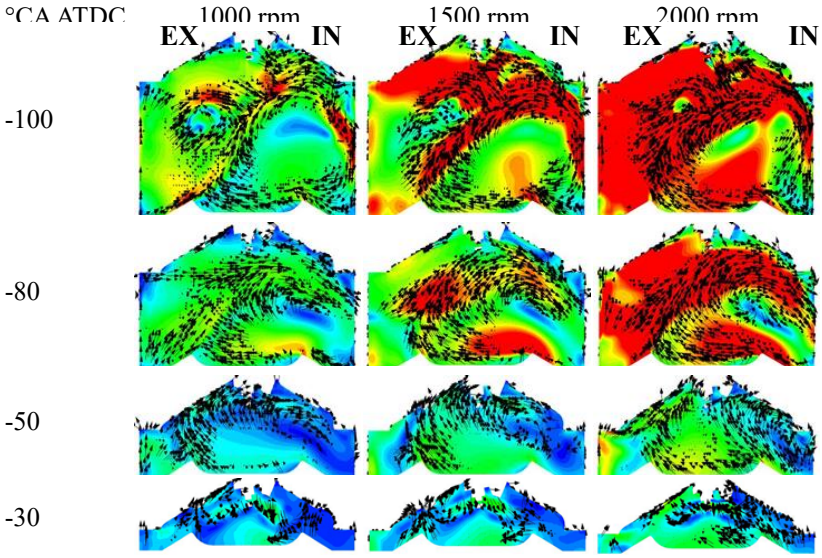


(a)

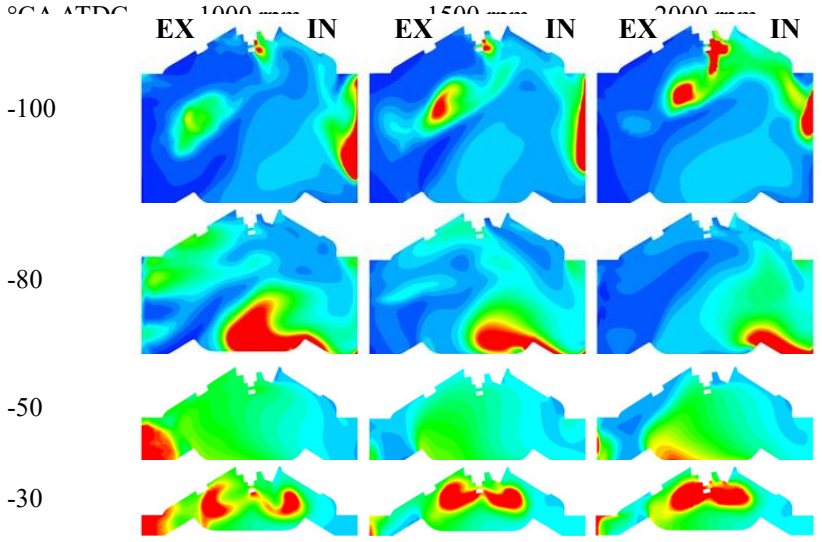


(b)

Fig. 7. The distribution of velocity (a) and equivalence ratio (b) of the mixture in the clip plane S1.

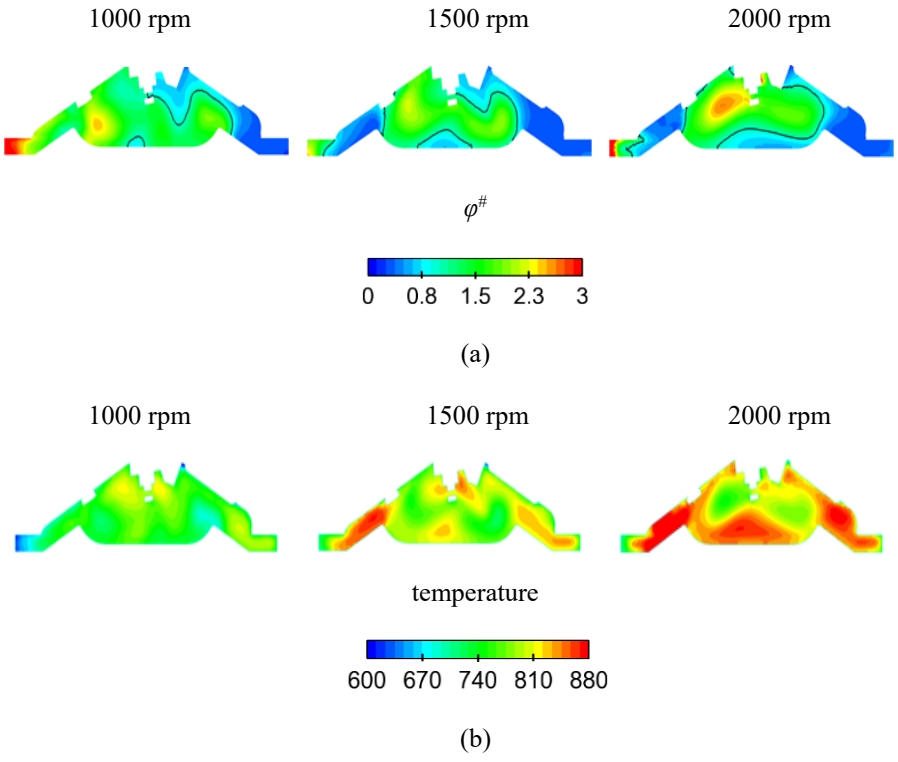


Fig. 8. The distribution of $\varphi^{\#}$ (a) and temperature (b) of the mixture in the clip plane S1 at -20°CA ATDC.

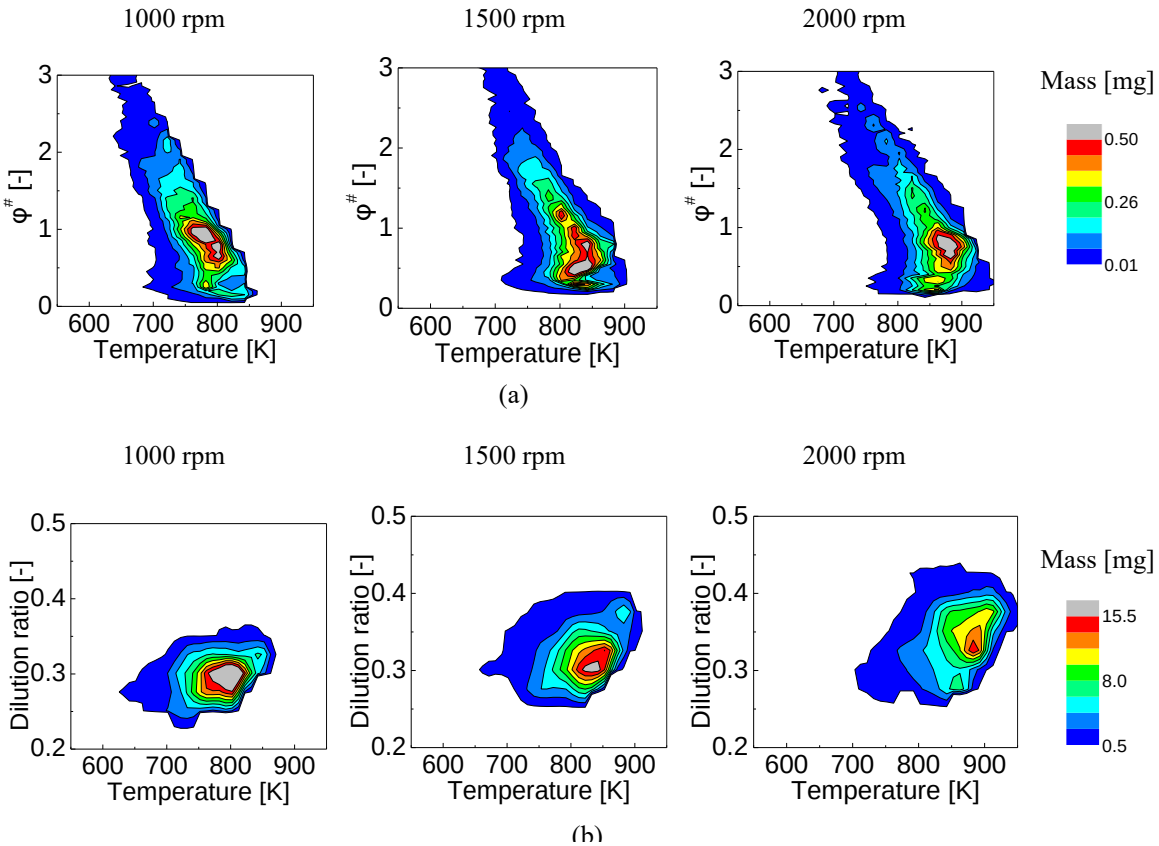


Fig. 9. The mass distribution of fuel-air mixture with temperature and $\varphi^{\#}$ (a)/dilution ratio (b) in the cylinder at spark timing at different engine speeds.

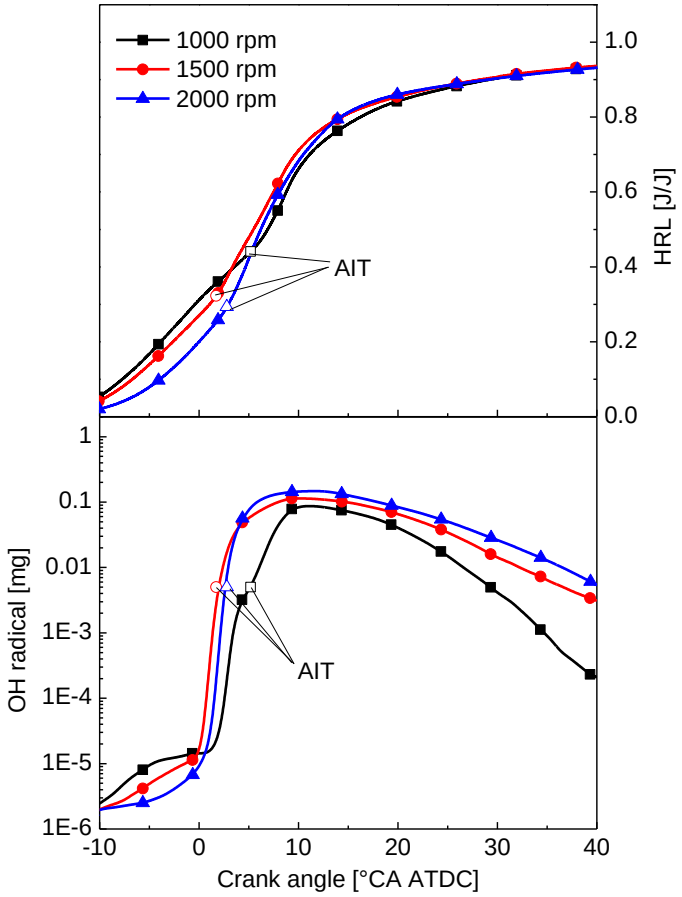


Fig. 10. OH radical in the peripheral zone prior to flame front and HRL at different speeds.

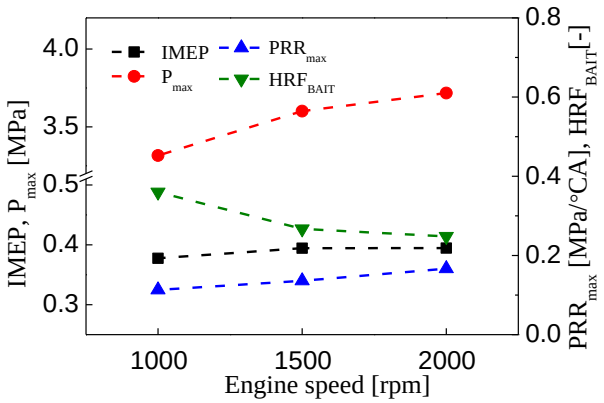


Fig. 11. Comparison of *IMEP*, $PRR_{max}$ , $P_{max}$ and $HRF_{BAIT}$ at different engine speeds.

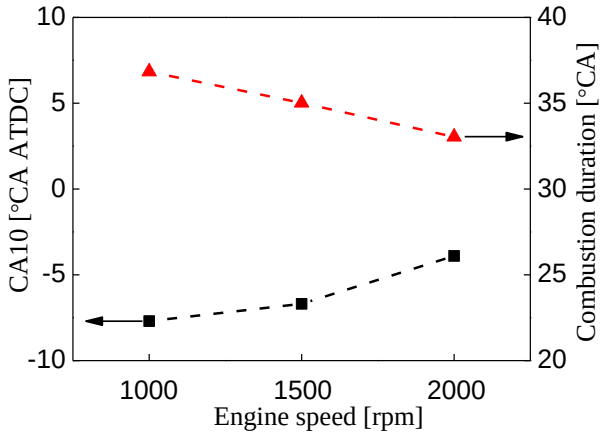


Fig. 12. Comparison of *CA10* and combustion duration at different engine speeds.

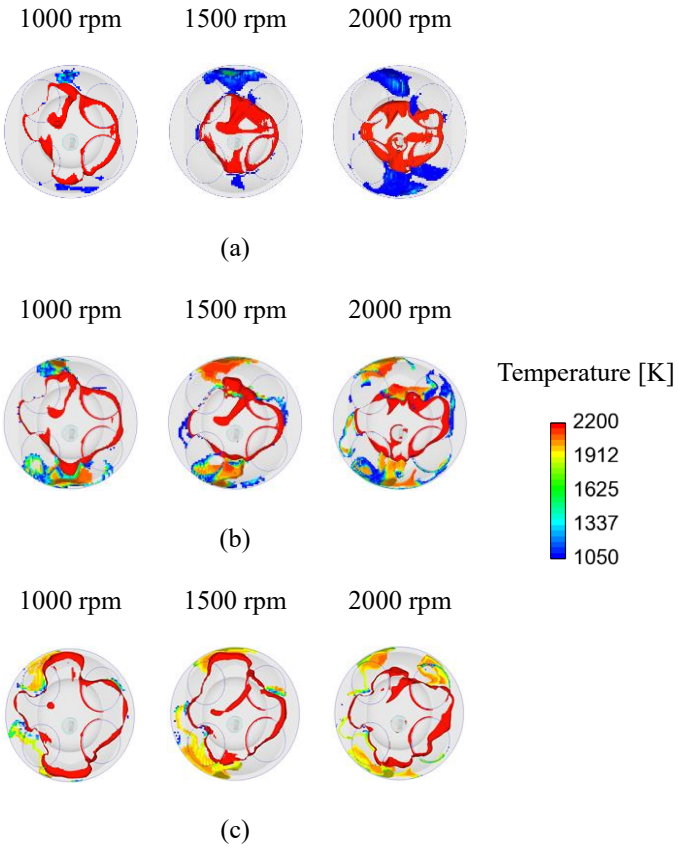


Fig. 13. Temperature distribution in the cylinder at AIT (a), 10°CA ATDC (b) and 20°CA ATDC (c) at different engine speeds.